63-3-1

SECOND QUARTERLY TECHNICAL NOTE

on a

STUDY OF MULTI-FUNCTION SENSORS FOR GUIDANCE SUBSYSTEMS

Prepared by

Alan Bloch

GENERAL PRECISION, INC.

Tarrytown, New York

April 1963

Contract No. AF33(657)-9207

Aeronautical Systems Division

Wright-Patterson Air Force Base

Ohio

NOTICES

When Government drawings, specifications, or other data are used for any purpose other than in connection with a definitely related Government procurement operation, the United States Government thereby incurs no responsibility nor any obligation whatsoever; and the fact that the Government may have formulated, furnished, or in any way supplied the said drawings, specifications or other data, is not to be regarded by implication or otherwise as in any manner licensing the permission to manufacture, use or sell any patented invention that may in any way be related thereto.

Qualified requesters may obtain copies of this report from the ASTIA Document Center, Arlington Hall Station, Arlington 12, Virginia. ASTIA Services for the Department of Defense contractors are available through the "Field of Interest Register" on the "need-to-know" certified by the cognisant military agency of their project or contract.

ASTIA Document No. AD-

SECOND QUARTERLY TECHNICAL NOTE

on a

STUDY OF MULTI-FUNCTION SENSORS FOR GUIDANCE SUBSYSTEMS

Prepared by
Alan Bloch

GENERAL PRECISION, INC.
Tarrytown, New York

April 1963

Contract No. AF33(657)-9207

Aeronautical Systems Division
Wright-Patterson Air Force Base
Ohio

FOREWORD

This report was prepared by General Precision, Inc., Tarrytown, New York, on Contract AF33(657)-9207, Project Nr. 4427 with the Aeronautical Systems Division, Wright-Patterson Air Force Base, Ohio. The work was administered under the direction of Mr. C. Coombs of ASD.

The work reported herein covers the period from 1 October, 1962 to 31 December, 1962 and was performed under the direction of A. Bloch, Program Manager for GPI. Principal contributors were L. Goldfischer and A. Miccioli of GPL and W. Davis of Librascope.

This report covers the second quarter of a one year program ending 30 June, 1962.

ABSTRACT

The purpose of the program detailed herein is the ultimate development of multi-function sensors for space-vehicle guidance and navigation. This second quarterly report contains detailed discussions of the work carried out by the contractor during the reporting period. A section is devoted to the theory of Fresnel zone plates. Plans for the next quarter are discussed briefly.

TABLE OF CONTENTS

LIST OF ILLUSTRATIONS

1. INTRODUCTION

The broad objective of the work reported here is, ultimately, the development of one or more multi-function sensors for space-vehicle guidance and navigation. The more limited objective of the present contract is the development of concepts and preliminary designs in terms of their suitability for possible further development work.

Although the use of multi-function sensors offers some possibility of reduction in over-all system size, weight, and power consumption, the primary reason for developing these sensors is the promise of improvement in over-all system reliability. A single multi-function sensor may or may not be preferable to the equivalent set of special-purpose sensors. A redundant set of multi-function sensors, however, is almost certain to offer higher reliability than the equivalent non-redundant set of special-purpose sensors.

Another way of improving system reliability is through reduction in the computing load. For example, a multi-function sensor might stabilize itself (function 1) by locking on to the celestial sphere (star-field tracking) and simultaneously track a target (function 2) directly in celestial coordinates. The alternative straightforward approach involves star-field or multiple-star tracking to determine vehicle orientation, target tracking in a vehicle coordinate system, and computation to convert the observed (body-axis) target coordinates to absolute (celestial) target coordinates.

For the present, at least, the program is limited to the field of optical sensors --- but with no restriction to the visible portion of the spectrum. A further limitation of the initial work is that the sensor functions considered should be appropriate to operation in cis-lunar space.

Two sorts of multi-function sensors come immediately to mind. One is a GPL correlator with presently-available terrain-matching capability and with, at least, added star-field tracking capability. The other is a combination of TV pickup and edge-sensing capabilities, making use of Librascope techniques. Most of the work during this quarter was oriented toward the first of these.

2. BACKGROUND

By the end of the last quarter it was apparent that one interesting possibility for a multi-function sensor might be a combination of the existing terrain-matching capability of the GPL correlator with the star-field tracking capability under development. On this basis, one obvious area for effort in the second quarter was that of bringing the star-field tracking capability up to a level approximating that of the terrain-matching capability.

It was tentatively decided during the first quarter that the program would aim primarily at exploitation of the GPL correlation technique to the exclusion of the Librascope technique. One reason for this decision was the relative simplicity of the GPL technique. Another reason was the fact that the Librascope technique is presently undergoing further development and refinement under other contracts. A second area for work during the second quarter was that of further consideration of this decision with a view to confirmation of our earlier conclusion.

On the assumption that the program would finally be strongly oriented toward the development of star-field tracking capability for the GPL correlator, there were a number of unresolved questions at the end of the first quarter.

a) Can the GPL correlator look directly at the star field (as the terrain-matching version looks directly at the ground), or will sensitivity limitations impose a requirement for electronic image intensification?

b) If image intensification is required, should this be post-correlation or pre-correlation?

c) If pre-correlation image intensification is used, should additional functions be allocated to the optical front end (image translation, etc.)?

d) Is it possible, in the present state of the art, to design an electronic equivalent of a mechanical gimbal system? Such a system would eliminate the requirement for many of the moving parts in the GPL correlator.

In the light of these outstanding questions, and of the decision to press on with development of the star-field tracking capability, the second quarter program was directed toward two major and two minor objectives.

a) A major effort, at GPL, was devoted to further development of the star-field reference.

b) A minor effort, at GPL, was devoted to the question of characteristics and energy levels of typical spectral star-field targets.

c) A major effort, at Librascope, was devoted to ascertaining the state of the art in the field of optical/electronic transducers.

d) A minor effort, at Librascope, was devoted to the specific question of the possibility of developing the electronic equivalent of a gimballing system.

Detailed results of the work in these areas are discussed in the following section of this report.

3. WORK DURING THE CURRENT QUARTER

Work during the current quarter (October, November, December 1962) was essentially in accordance with the four-pronged effort mentioned in the preceding section. Significant progress was made in each of these areas.

3.1 Star-Field Reference

By the end of the last quarter significant work had been accomplished toward two types of star-field references. One of these consists of a photograph of a set of Fresnel zone plates, one for each star. The other consists of a spherical metal shell carrying a separate lens for each star.

3.1.1 Zone-Plate Reference

Fabrication of a successful zone-plate reference for use with a simulated star field obviously depends on the availability of Fresnel zone plates of suitable size and focal length. By the end of the last quarter, fabrication techniques had been advanced to the point of successfully producing a Fresnel zone plate with a focal length of 8 inches having 100 zones in a 1/4 inch diameter. Fired by this success, GPL proceeded to develop techniques for fabricating zone plates with a focal length of 8 inches having 400 zones in a 1/2 inch diameter.

The superior performance inherent in the 400-zone Fresnel plate, as compared to the 100-zone model, is considerable and justifies the new effort. A four-fold increase in light gathering capacity is anticipated as a result of doubling the diameter. In addition, again due to doubling the diameter, the area of the image spot will be reduced by a factor of four. The combined result of these two effects is expected to be an increase by a factor of 16 in brightness (lumens per unit area)

of the image spot compared to that achievable with the 100-zone plate.

Even more significant is the fact that the theoretical brightness of the image spot with a 400-zone 1/2 inch Fresnel plate is 61% greater than that which may be achieved with a conventional 1/4 inch lens. Overlapping zone plates when used in a star-field reference will, of course, reduce this improvement somewhat. On the other hand, however, it is expected that the number of stars which may be represented on the reference will not be physically limited as will be the case if conventional lenses are employed. Hence, successful development of a 400-zone plate should provide the possibility of a Fresnel zone plate reference which compares favorably with a lensed version.

Previously reported zone plates were first drawn to large scale and then photographically reduced. The dimensions and tolerances associated with the outer rings of a 400-zone plate preclude the use of art work, but are within the capabilities of machining operations. Therefore the large scale model for the 400-zone plate was machined from a black-anodized aluminum jig plate. The result was an 18 inch diameter master zone plate having 400 alternate black and aluminum zones.

Initial attempts to fabricate the desired 1/2 inch zone plate in the laboratory by double photographic reduction from the 18 inch master were not successful. However, successful results were obtained by the GPL Photo Lab, using equipment of higher precision. An experimental star-field reference was then fabricated using 20 of the 1/2 inch Fresnel zone plates positioned to represent the brightest stars in a region of the sky around Polaris. This reference will be tested in the laboratory against a star-field simulator which contains a large number of stars (20 of which are those associated with the reference) from the same celestial region.

The central diffraction image formed by a Fresnel zone plate lies in a background of light which passes through the zone plate without being diffracted. By blocking out the central portion of the zone plate, it is possible to effect a sharp reduction in the background (near the center of the field) while reducing the intensity of the diffraction image only slightly. This effect was verified on a single zone plate and a second star-field reference was fabricated using modified Fresnel plates (with opaque centers). As expected, the signal-to-background ratio of the central spot in the star-field correlation image was markedly enhanced.

Attempts were made, using a point detector, to make a quantitative investigation of the pattern formed by overlapping zone plates. This work was started late in the present quarter, and no significant results were obtained. It will be continued in the next quarter.

A discussion of the theory of the Fresnel zone plate has been prepared and is incorporated in this report as Appendix A.

3.1.2 Lensed Reference

The spherical shell for a lensed reference was fabricated during this quarter. This reference models the same region of the sky as the Fresnel plate reference described above.

3.1.3 Other References

Consideration was given to the possibility of fabricating a lensed reference by plastic molding, but it was decided not to expend any effort in this direction.

3.2 Spectral Characteristics of Star Fields

Some work was done at GPL in the general area of spectral characteristics and energy levels of typical star fields at which

the star-field tracker might look. The immediate outcome of this study is a conclusion that the state of the art in detector sensitivity is such that some sort of image intensification will be required to provide the GPL correlator with a star-field tracking capability.

The results of this study are included as Appendix B of this report. The study itself was very brief and is only a first pass at the problem. Its aim, however, was merely to provide an answer to the question of whether or not image intensification will be required. For this purpose it is adequate.

3.3 Survey of Optical Front-Ends

A moderately comprehensive survey of optical/electronic transducers was made by the Librascope Division. As a result of this study, the following conclusions were reached.

a) Adequate light amplification is available to make star-field tracking feasible for the GPL correlator.

b) The resolution of available image intensifiers is such that they should be employed in a post-correlation configuration.

c) Because of relatively poor resolution and linearity, electronic image manipulation should be considered as beyond the present state of the art. On this basis, the GPL correlator should look directly at its targets and should employ post-correlation image intensification as required.

d) Further, because of poor resolution and linearity, the precision available from the Librascope correlation technique is probably inferior, at present, to that available from the GPL technique. The Librascope approach will, however, be useful in areas where straightforward image correlation is not applicable —— edge sensing and TV pickup in particular —— and current development of the technique

will be followed.

An abbreviated report of the Librascope work is included as Appendix C.

3.4 Electronic Gimballing

As a result of the study discussed above, it was decided that any comprehensive attempt at electronic gimballing is beyond the present state of the art. No further work will be done in this area.

4. PLANS FOR THE NEXT QUARTER

Plans for the coming quarter (January, February, March 1963) are briefly outlined below.

GPL Work will be continued in the general area of the star-field tracker with emphasis on the Fresnel zone plate reference. In particular, experimental and theoretical studies of the behavior of overlapping zone plates are contemplated.

GPL A short study will be made covering the possibility of nonstandard operation of the GPL correlator. One area of interest is the possibility of manual operation by an operator to whom suitable error signals are displayed. Another area of interest is the possibility of developing two sets of error signals (appropriately labeled by modulation) — one set to be used for stabilizing the instrument, and a second set to be used for tracking a cooperating target.

GPL Consideration will be given to the general problem of tracking a cooperative vehicle for the purpose of effecting rendezvous. It is hoped that justification can be developed for tracking such a vehicle directly in absolute (celestial) coordinates.

Librascope Some work will be carried out in the area of star-field spectra and energy levels, backing up the first pass which is included as Appendix B of this report.

Librascope A brief report will be prepared covering recent work on the pass-point instrument and contour plotter. This will supplement Appendices B and C of the First Quarterly Report.

APPENDIX A

FOCUSSING PROPERTIES OF FRESNEL ZONE PLATES

A diagram of a Fresnel zone plate appears in Figure 1. Opaque zones (zero transmission) are shown hatched while clear zones (unity transmission) are unhatched. The radii of the transitions from clear to opaque and vice-versa are chosen to make the difference in path lengths from the focal point of the zone plate to the two edges of any zone equal to one half wavelength at the operating frequency. Numbering the transitions as in Figure 1, the radius of the m^{th} transition, r_m, is calculated from the relationship

$$\sqrt{f^2 + r_m^2} - f = \frac{m\lambda}{2} \tag{1}$$

where the factor in the radical is the path length from the m^{th} transition to the focal point, f is the focal distance and λ is the wavelength of operation. In a practical zone plate

$$f \gg r_m \tag{2}$$

for all values of m, leading to the approximation

$$\sqrt{f^2 + r_m^2} = f\sqrt{1 + (r_m/f)^2} \approx f\left\{1 + \frac{r_m^2}{2f^2}\right\} \tag{3}$$

Applying this approximation to (1) yields

$$\frac{m\lambda}{2} = \frac{r_m^2}{2f} \tag{4}$$

or

$$r_m = \sqrt{m\lambda f} \tag{5}$$

The area of each zone is very nearly the same as that of any other zone, as can be seen by calculating the area between transitions m and m-1. This is

$$\pi(r_m^2 - r_{m-1}^2) = \pi(mf\lambda - [m-1]\, f\lambda) = \pi f\lambda \tag{6}$$

where use was made of the approximation in (4).

The illuminance at the focal point of the zone plate is determined by squaring the vector sum of the contribution from each clear zone. Since all clear zones have very nearly the same area, and are (for a practical zone plate) at virtually the same distance from the focal point, the contribution of each zone will have the same magnitude. The construction of the zone plate assures that all zonal contributions will add in phase (the opaque zones block out the out of phase contributions). Hence, if the vector contribution of the first zone is k and there are n clear zones, the total vector magnitude at the focal point will be nk.

The vector contribution of the first zone may be found on the basis of a rather simple argument due to Fresnel. Imagine that the zone plate is replaced by a variable iris which is first closed down to the diameter of the first zone and then opened in steps so that its circumference coincides with the next larger zone transition at each step. Let the iris be illuminated with axial columated light and observe the magnitude of the vector intensity at each step. At the first step, the magnitude will be k and at the second step it will be nearly zero. In general, the magnitude will rise on each odd numbered step because of the addition of the contribution of a zone in phase with the first zone and will fall on each even numbered step because of the contribution of an out of phase zone. However, each rise and fall will be slightly less than the one preceding it because of the obliquity factor $(1 + \cos \theta)$, where θ is the angle between the incident illumination and the direction from a given zone to the focal point. (The obliquity factor combined with Huygens' construction insures that light will be propagated only in the foreward direction.) Since the obliquity factor varies slowly, a plot of the vector magnitude as a function of step number would appear to oscillate with diminishing amplitude around the value k/2. This is illustrated in Figure 2.

When the iris opening becomes indefinitely large, the vector intensity at the focal point becomes k/2 and the illuminance at that point becomes identical with the incident illuminance, I. Hence

$$\frac{k^2}{4} = I \tag{7}$$

and the illuminance at the focal point of a zone plate with n clear zones is

$$I_z = n^2 k^2 = 4n^2 I \tag{8}$$

where I is the incident illuminance on the zone plate.

The diffraction pattern appearing at the focal point of the zone plate when illuminated by an axial plane wave is analyzed on the basis of the geometry of Figure 3. The vector intensity at any point in the focal plane, at a displacement y_o from the focal point is

$$V = \frac{C}{\pi R^2} \int_0^R \rho\, S(\rho)\, d\rho \int_0^{2\pi} \exp\left[\frac{2\pi j}{\lambda}\left(\frac{\rho^2 - 2\rho\, y_o \sin\theta}{2f}\right)\right] d\theta \qquad (9)$$

where C is a constant to be adjusted in conformation with (8),
R is the outermost radius of the zone plate
S(ρ) is the transmission of the zone plate along a radius and is given by

$$S(\rho) = \left\{\begin{array}{l} 1,\ \sqrt{m\lambda f} \leq \rho \leq \sqrt{(m+1)\lambda f} \\ \\ 0,\ \sqrt{(m+1)\lambda f} \leq \rho \leq \sqrt{(m+2)\lambda f} \end{array}\right\} \quad m = 0, 2, 4, \ldots$$

If the function S(ρ) were plotted as a function of ρ^2, it would be seen to be a square wave with a 50% duty ratio, peak to peak excursion of unity and average value of one half. Hence, it may be expanded in a Fourier series with ρ^2 as the variable and with a period of 2 λf to yield

$$S(\rho) = \frac{1}{2} + \frac{2}{\pi}\left\{\sin\frac{\pi\rho^2}{\lambda f} + \frac{1}{3}\sin\frac{3\pi\rho^2}{\lambda f} + \cdots\right\}$$

$$= \frac{1}{2} + \frac{1}{\pi}\sum_{k=-\infty}^{\infty} \frac{1}{(2k-1)\,j} \exp\left[(2k-1)\, j\pi\, \rho^2/\lambda f\right] \qquad (10)$$

Substituting from (10) into (9) and rearranging yields

$$V = \frac{C}{\pi R^2} \int_0^R \rho \left\{\frac{\exp\left[j\pi\rho^2/\lambda f\right]}{2} - \frac{j}{\pi}\sum_{k=-\infty}^{\infty} \frac{\exp\left[j2k\pi\rho^2/\lambda f\right]}{2k-1}\right\} d\rho$$

$$\cdot \int_0^{2\pi} \exp\left[-j2\pi\rho y_o \sin\theta\, /f\lambda\right] d\theta \qquad (11)$$

The kernel of the second integral may be expanded into a series with Bessel function coefficients as below:

$$\exp\left[-j\frac{2\pi\rho\, y_o \sin\theta}{f\lambda}\right] = J_o\left(\frac{2\pi\rho\, y_o}{f\lambda}\right) + 2\sum_{q=1}^{\infty} J_{2q}\left(\frac{2\pi\rho\, y_o}{f\lambda}\right)\cos 2\theta$$

$$- 2j\sum_{p=1}^{\infty} J_{2p-1}\left(\frac{2\pi\rho\, y_o}{f\lambda}\right)\sin(2p-1)\theta \qquad (12)$$

Hence, the second integral reduces to

$$\int_0^{2\pi} \exp\left[-j\frac{2\pi\rho y_o \sin\theta}{f\lambda}\right] d\theta = 2\pi J_o\left(\frac{2\pi\rho y_o}{f\lambda}\right) \qquad (13)$$

Now, substituting from (13) into (11) yields

$$V = -\frac{2jC}{\pi R^2}\int_0^R \rho\, J_o\left(\frac{2\pi\rho y_o}{f\lambda}\right) d\rho + \frac{C}{R^2}\int_0^R \rho \exp\left[\frac{j\pi\rho^2}{\lambda f}\right] J_o\left(\frac{2\pi\rho y_o}{\lambda f}\right) d\rho$$

$$- \frac{2jC}{\pi R^2}\int_0^R \rho \sum_{k=1}^{\infty} \frac{\exp(j2k\pi\rho^2/\lambda f)}{2k-1} \cdot J_o\left(\frac{2\pi\rho y_o}{\lambda f}\right) d\rho$$

$$- \frac{2jC}{\pi R^2}\int_0^R \rho \sum_{k=-1}^{-\infty} \frac{\exp(j2k\pi\rho^2/\lambda f)}{2k-1} \cdot J_o\left(\frac{2\pi\rho y_o}{\lambda f}\right) d\rho \qquad (14)$$

In the vicinity of the focal point ($y = o$) the first term on the right side of (14) is dominant and the others may be neglected. The justification involves the fact that $J_o(\epsilon) \approx 1$ when ϵ is small (as it is when $y_o \approx o$) and that the exponential quantities in the last three terms oscillate many times over the range of integration yielding integrals which are nearly zero. Hence

$$
\begin{aligned}
V(y_o) &= -\frac{2jC}{\pi R^2} \int_o^R \rho\, J_o\left(\frac{2\pi\rho y_o}{f\lambda}\right) d\rho \\
&= -\frac{2jC}{\pi R^2} \cdot \left(\frac{f^2\lambda^2}{4\pi^2 y_o^2}\right) \int_o^R \left[\frac{2\pi\rho y_o}{f\lambda} J_o\left(\frac{2\pi\rho y_o}{f\lambda}\right) \frac{2\pi y_o}{f\lambda}\right] d\rho \\
&= -\frac{2jC}{\pi R^2} \left(\frac{f^2\lambda^2}{4\pi^2 y_o^2}\right) \left[\frac{2\pi y_o \rho}{f\lambda} J_1\left(\frac{2\pi y_o \rho}{f\lambda}\right)\right]_o^R \\
&= -\frac{2jC}{\pi R^2} \left(\frac{f\lambda}{2\pi y_o}\right) \cdot R\, J_1\left(\frac{2\pi y_o R}{f\lambda}\right)
\end{aligned}
\qquad (15)
$$

If the zone plate contains n clear zones

$$R = \sqrt{(2n+1)\, f\lambda} \qquad (16)$$

Therefor

$$V(y_o) = -\frac{2jC}{\pi} \frac{J_1\left(2\pi y_o \sqrt{2n+1} \,/\, \sqrt{f\lambda}\right)}{\left(2\pi y_o \sqrt{2n+1} \,/\, \sqrt{f\lambda}\right)} \qquad (17)$$

The constant C is evaluated by setting

$$|V(o)|^2 = 4n^2 I \qquad (18)$$

from (8). Substituting from (17) into (18) yields

$$\frac{4C^2}{\pi^2}\left[\frac{J_1(o)}{(o)}\right]^2 = \frac{4C^2}{\pi 2} \cdot \frac{1}{4} = 4n^2 I$$

$$\text{or } C^2 = 4\pi^2 n^2 I \tag{19}$$

Hence the diffraction pattern in the focal plane is given very nearly by

$$|V(y_o)|^2 = 16n^2 I \left[\frac{J_1\left(2\pi y_o \sqrt{2n+1} \,/\, \sqrt{f\lambda}\right)}{\left(2\pi y_o \sqrt{2n+1} \,/\, \sqrt{f\lambda}\right)}\right]^2 \tag{20}$$

A plot of equation (20), normalized to the value at the peak, appears in Figure A-4. The main lobe of the diffraction pattern is seen to be more than 20 times brighter at the peak than the maximum brightness of the first minor lobe.

The first zero of the $J_1(x)/x$ function occurs when $x = 3.83$. Hence, the main lobe of the diffraction pattern is confined within a radius, r_d, given by

$$\frac{2\pi r_d \sqrt{2n+1}}{\sqrt{f\lambda}} = 3.83$$

$$r_d = \frac{3.83}{2\pi}\sqrt{\frac{f\lambda}{2n+1}} = 0.625\sqrt{\frac{f\lambda}{2n+1}}$$

$$= 0.625\frac{\sqrt{(2n+1)\,f\lambda}}{2n+1} = 0.625\frac{R}{2n+1}$$

$$\text{or} \quad \frac{r_d}{R} = \frac{1}{3.2n} \tag{21}$$

This result, i.e. the shape and size of the diffraction pattern, is identical with what would have been the case if a lens of radius R and focal length f had been used in place of the zone plate. However, the light gathering power of the lens is greater than that of the zone plate. All of the light incident on the lens appears in a diffraction pattern like that given by (20). The zone plate rejects half of the incident

light immediately (by virtue of the opaque zones) and places part of the remainder into non-focussing diffraction orders. This is the significance of the terms of (14) which were neglected in arriving at (20). The first neglected term represents a portion of the incident plane wave propagating straight through the zone plate, attenuated by the average transmission alone. The remaining neglected terms represent waves converging to real foci at f/3, f/5 etc. and diverging from virtual foci at -f, -f/3, -f/5, etc. The total power in each term, i.e. both the term representing power which comes to a focus at f and all other terms, is proportional to the square of the coefficient of the corresponding term in the complex expansion of $S(\rho)$ in (10). Since

$$\frac{1}{4} + \frac{1}{\pi^2} \sum_{k=1}^{\infty} \frac{1}{(2k-1)^2} = \frac{1}{2} \tag{22}$$

and since the square of the coefficient of the term which comes to a focus at f is

$$\left[\frac{1}{\pi^2 (2k-1)^2} \right]_{k=0} = \frac{1}{\pi^2}$$

the percentage of the incident power which appears in the dominant diffraction pattern is

$$\frac{1}{\pi^2} = 10.2\%$$

Hence, the zone plate has about one tenth the light gathering power of a lens of the same aperture. Conversely, a zone plate produces a diffraction image about ten times more concentrated than a lens of the same light gathering power. In addition, the zone plate being (in a sense) an infinitesimally thin lens, its off-axis focussing will be accomplished with significantly less aberrations than those encountered in a real lens.

The distribution of the power appearing in the dominant diffraction pattern is plotted in Figure A-5. The ordinate of each point on the curve gives the percentage of the total power (in the dominant pattern) that lies within a circle of radius x around the focal point. Here

$$x = 2\pi y_o \sqrt{\frac{2n+1}{f\lambda}}$$

and y_o is the actual radial distance in the focal plane. The curve in Figure A-5 was derived by integrating equation (20) over the focal plane and then normalizing by $1/\pi^2$ times the total power incident on the zone plate. Thus

$$\% \text{ total power} = \frac{2\pi \int_0^r |V(y_o)|^2 \, y_o \, dy_o}{\pi R^2 \, I/\pi^2}$$

$$= \frac{2\pi}{R^2 I} \cdot 4n^2 I \int_0^r y_o \left[\frac{2J_1(2\pi y_o R/f\lambda)}{(2\pi y_o R/f\lambda)}\right]^2 dy_o$$

$$= \frac{8\pi^2 n^2}{R^2} \left(\frac{f\lambda}{2\pi R}\right)^2 \int_0^x z \left[\frac{2J_1(z)}{z}\right]^2 dz$$

$$= \frac{2n^2}{(2n+1)^2} \int_0^x z \left[\frac{2J_1(z)}{z}\right]^2 dz$$

$$= \frac{1}{2} \int_0^x z \left[\frac{2J_1(z)}{z}\right]^2 dz \qquad (23)$$

In arriving at (23) liberal use was made of equation (16) relating R, n and $f\lambda$. Equation (2) was integrated numerically using the trapezoidal rule.

The plot in Figure A-5 shows that the main lobe contains approximately 84% of the power in the dominant diffraction pattern, while 50% of the power in this pattern is contained within a circle whose radius, r_h, is given by

$$2\pi r_h \sqrt{\frac{2n+1}{f\lambda}} = 1.74$$

$$r_h = \frac{1.74}{2\pi} \sqrt{\frac{f\lambda}{2n+1}} = \frac{0.277 \sqrt{f\lambda(2n+1)}}{2n+1}$$

$$= \frac{0.277 R}{2n+1}$$

or

$$\frac{r_h}{R} = \frac{1}{7.22n}$$

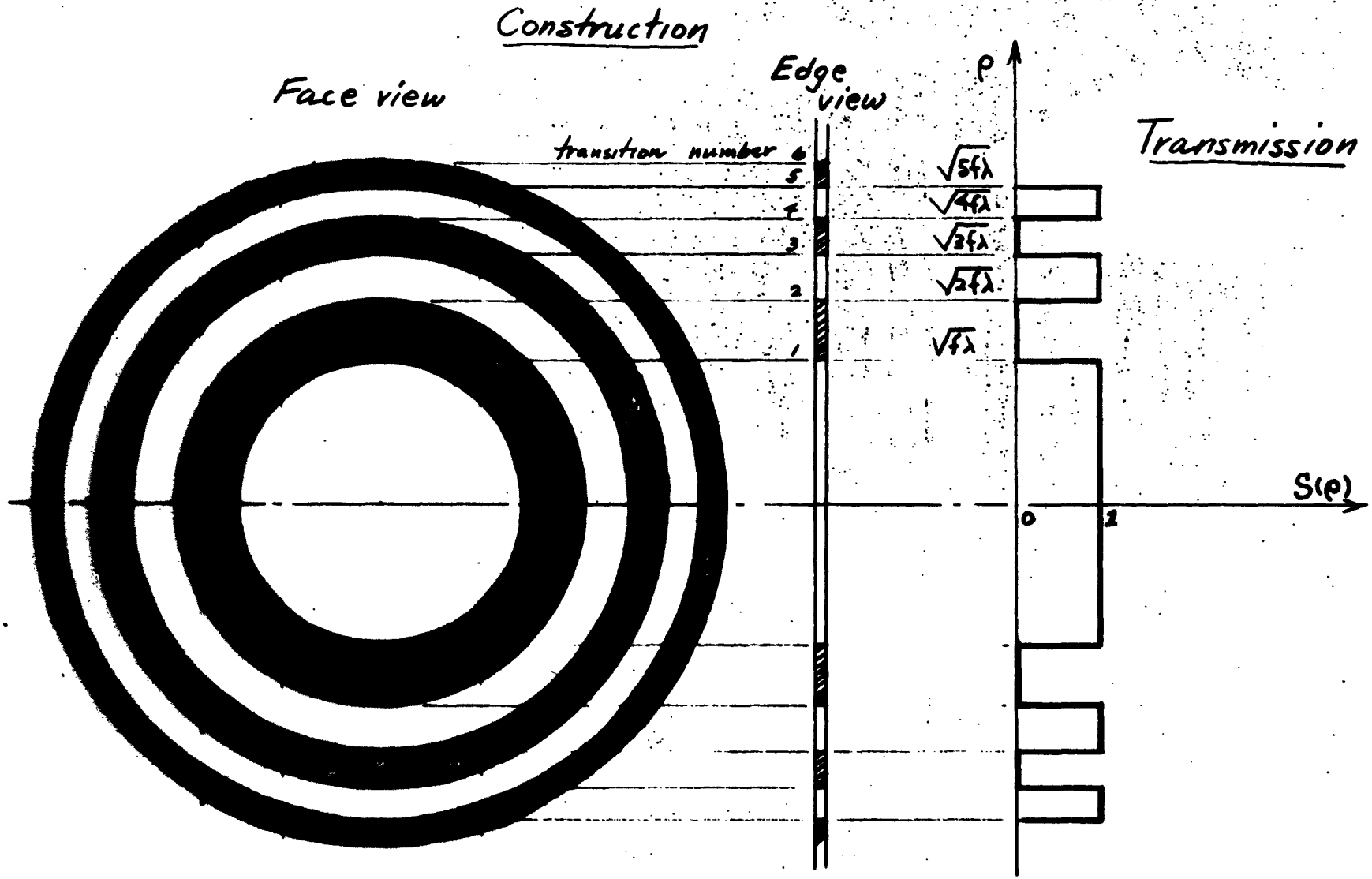

FIGURE A-1 ZONE PLATE LAYOUT

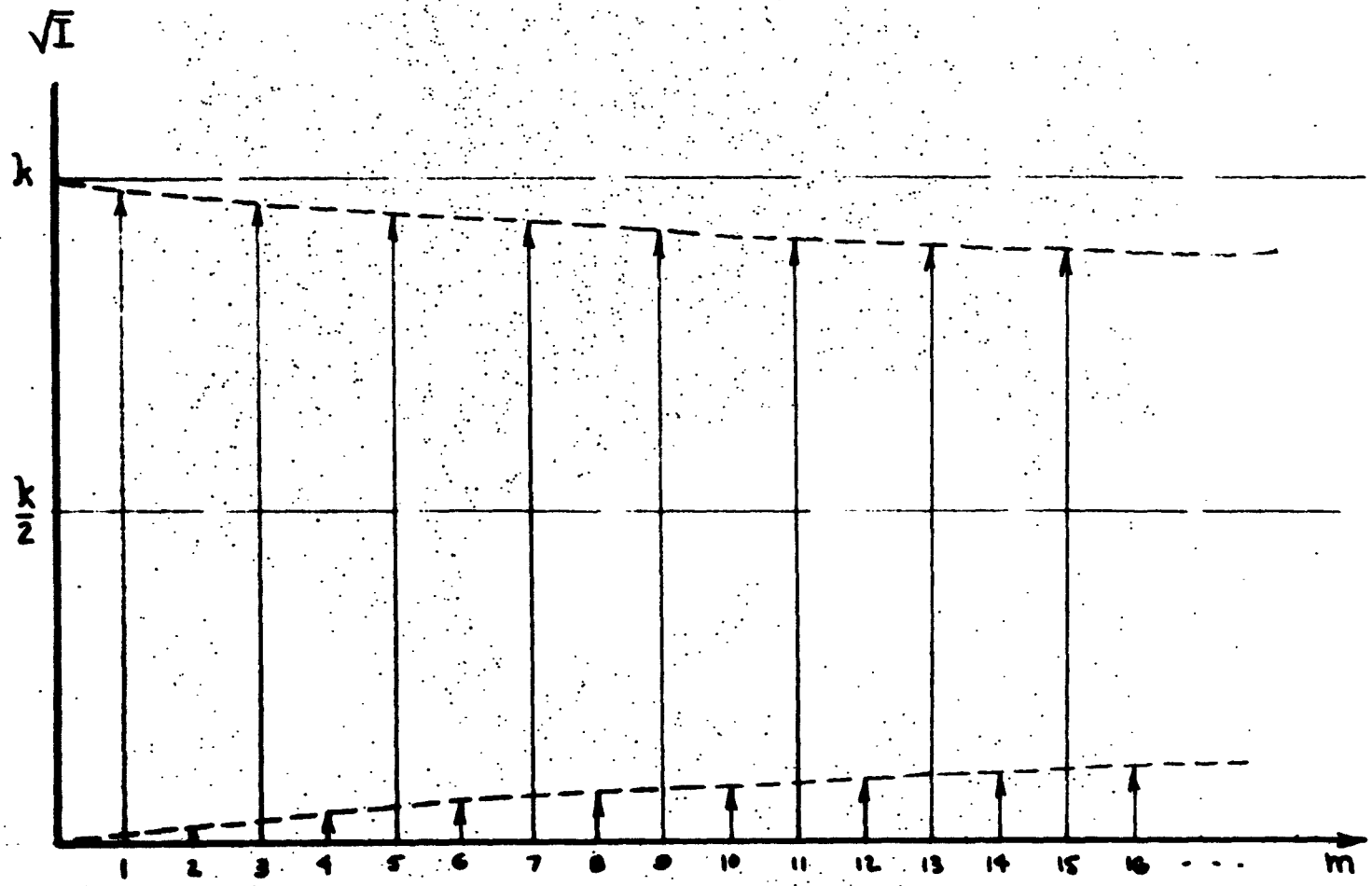

FIGURE A-2 VARIATION OF VECTOR INTENSITY AT THE FOCAL POINT AS A FUNCTION OF NUMBERS OF FRESNEL ZONES INCLUDED IN THE APERTURE

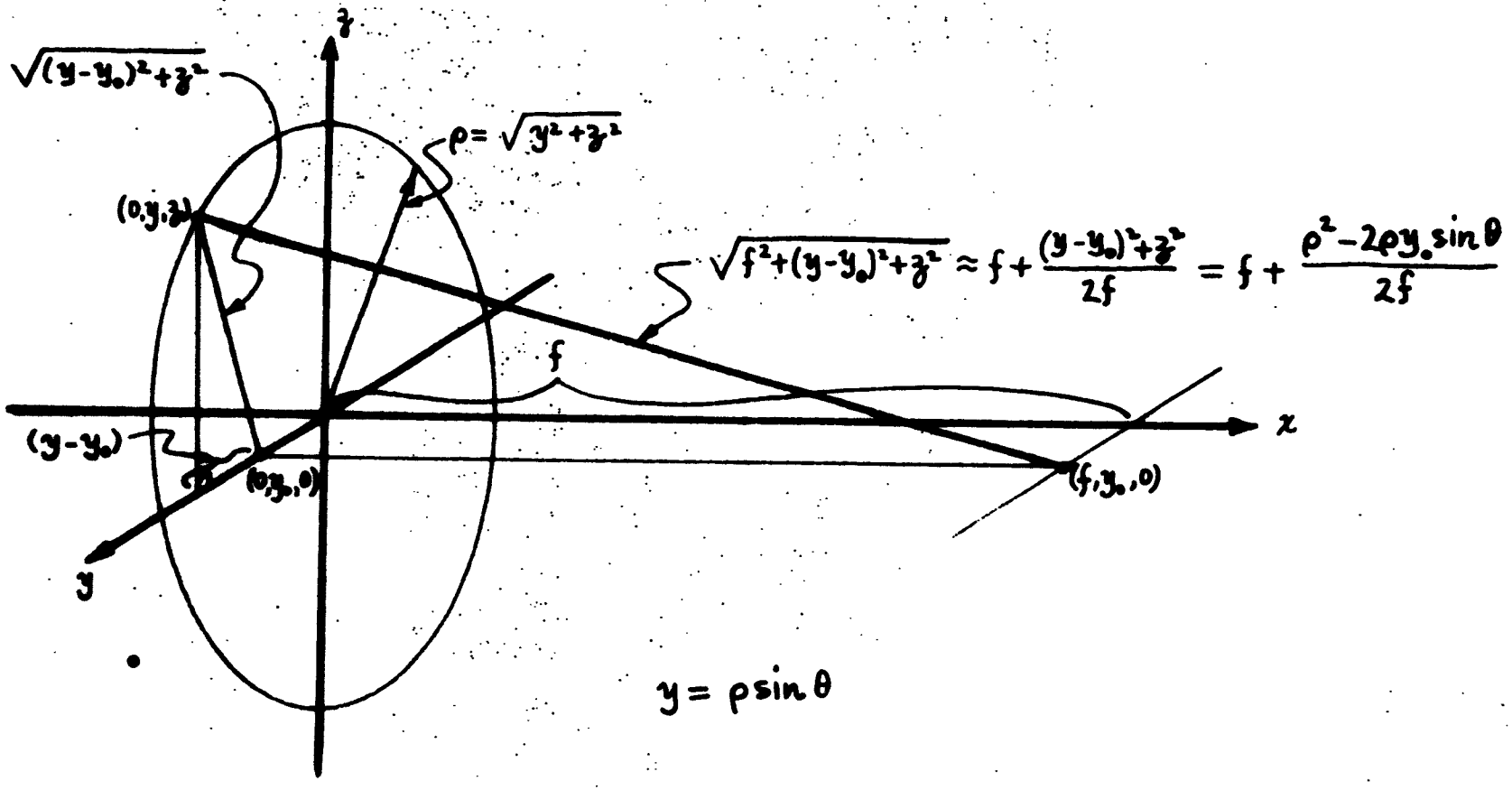

FIGURE A-3 GEOMETRY APPLICABLE TO DIFFRACTION CALCULATIONS

FIGURE A-4

DOMINANT DIFFRACTION PATTERN

FRESNEL ZONE PLATE

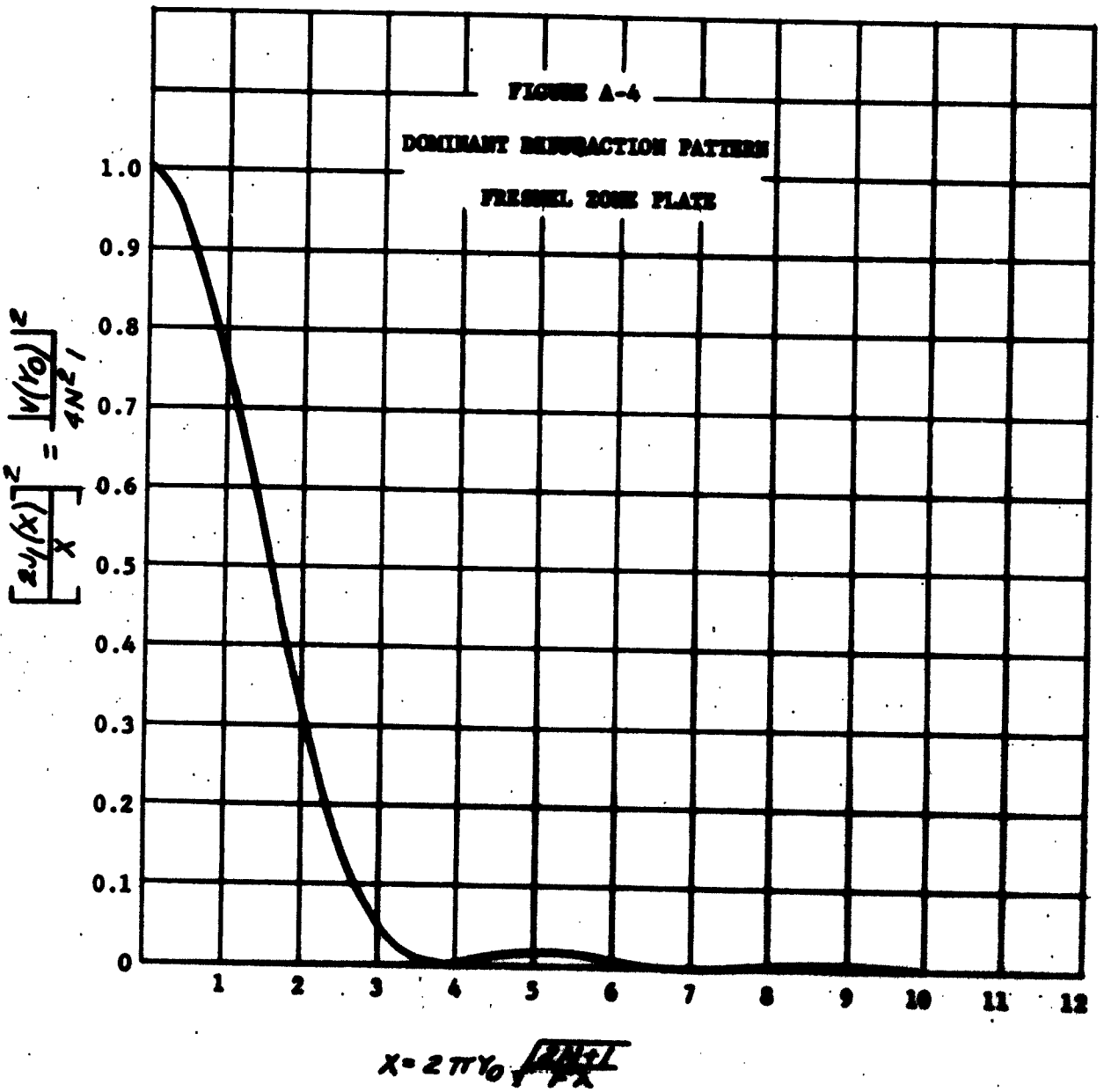

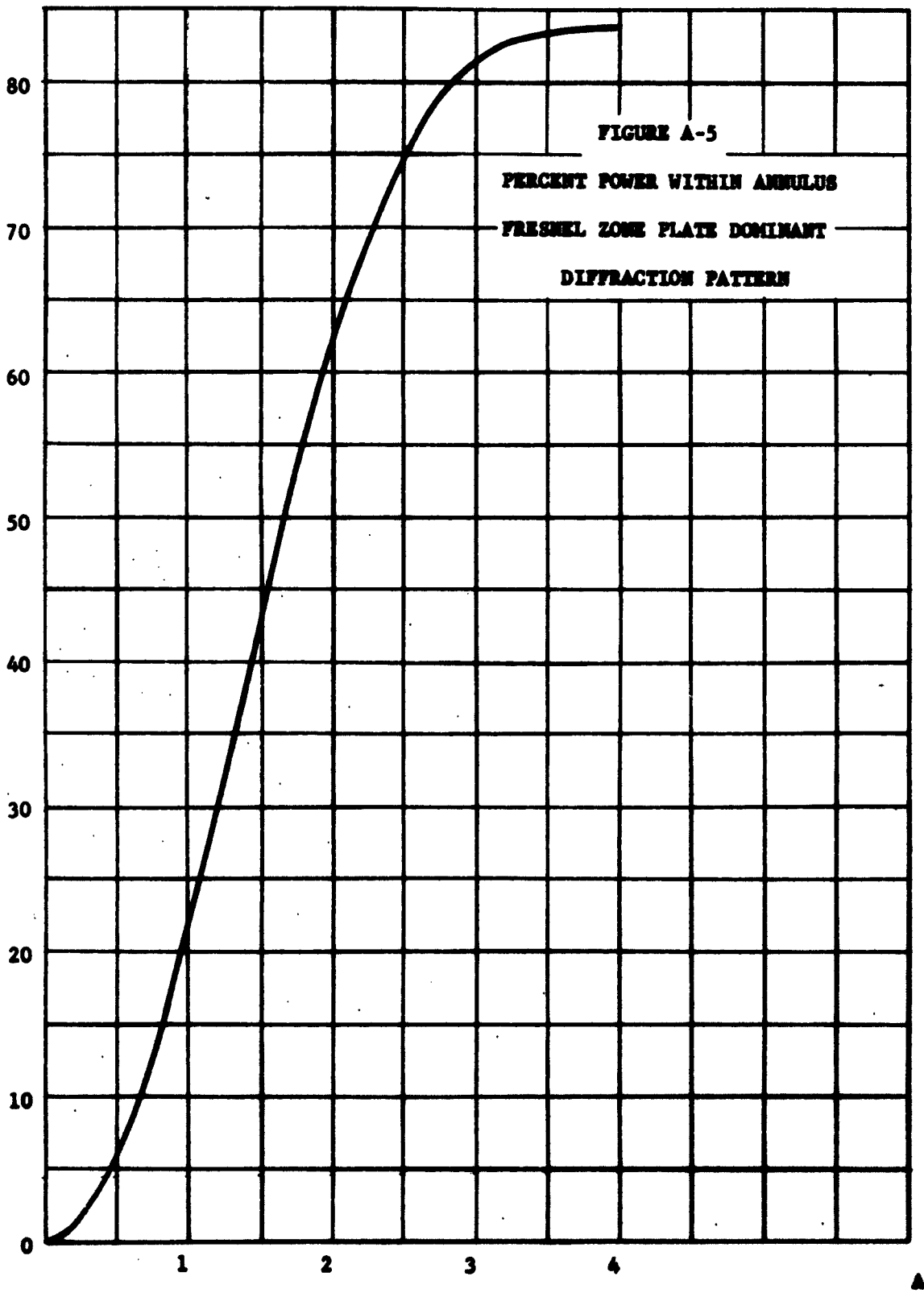

FIGURE A-5

PERCENT POWER WITHIN ANNULUS

FRESNEL ZONE PLATE DOMINANT

DIFFRACTION PATTERN

$x = \pi r_0 \sqrt{\frac{2N+1}{F\lambda}}$

APPENDIX B

AVAILABLE POWER FROM STARS

Selection of a suitable detector for star field tracking presupposes a knowledge of the spectral content of star light and the transmission characteristics of the lenses (either conventional lenses or Fresnel zone plate transparencies) as a function of wavelength. A detector with a spectral response which maximizes the relative system sensitivity can then be selected. Absolute system sensitivity would then be primarily a function of star statistics and would determine the need for image intensification.

Other factors must also be considered. The detector in a multi-function sensor must be compatible with more than one function. For example, it may be desired that the same detector be suitable for terrain matching as well as star field tracking. Then the spectral content of reflected sunlight from natural and man made objects must be considered in conjunction with the spectral content of star light.

Reference [1] indicates that there is little correlation between apparent brightness of a star and spectral type, and that more than 99 percent of the stars belong to spectral classes B, A, F, G, K, and M. By means of published data on the percentage of stars (from the Henry Draper Catalogue) of the principal spectral classes, the color temperature of stars of various spectral classes, and Planck's formula for the intensity of radiation of a black body as a function of wavelength, the spectral content of star light was estimated. Table 1 gives the results relative to the intensity at 0.1 micron. It should be noted that ultra violet radiation predominates.

TABLE I

Relative Spectral Content of Star Light

λ (microns)	0.01	0.1	0.2	0.3	0.4	0.5	0.6	0.7	0.8	0.9	1.0	1.1
E	4.1×10^{-20}	1	7.7×10^{-1}	3.6×10^{-1}	2.2×10^{-1}	1.3×10^{-1}	8.2×10^{-2}	5.8×10^{-2}	4.3×10^{-2}	3.1×10^{-2}	2.4×10^{-2}	1.8×10^{-2}

Star statistics have been briefly investigated during the past two months. The emphasis has been on galactic latitude 90 degrees

where the star density, number of stars per square degree, is a minimum. Based upon published data on star densities, the number of stars per square degree at galactic latitude 90 degrees as a function of visual magnitude has been calculated and is presented in Table II.

TABLE II

Star Densities as a Function of Visual Magnitude at Galactic Latitude 90 Degrees

M_v	-1/2 to 1/2	1/2 to 1 1/2	1 1/2 to 2 1/2	2 1/2 to 3 1/2	3 1/2 to 4 1/2	4 1/2 to 5 1/2	5 1/2 to 6 1/2	6 1/2 to 7 1/2	7 1/2 to 8 1/2
No/sq. deg.	6.32×10^{-5}	2.06×10^{-4}	8.35×10^{-4}	2.67×10^{-3}	1.04×10^{-2}	3.02×10^{-2}	7.78×10^{-2}	2.23×10^{-1}	6.04×10^{-1}
M_v	8 1/2 to 9 1/2	9 1/2 to 10 1/2	10 1/2 to 11 1/2	11 1/2 to 12 1/2	12 1/2 to 13 1/2	13 1/2 to 14 1/2	14 1/2 to 15 1/2	15 1/2 to 16 1/2	16 1/2 to 17 1/2
No/sq. deg.	1.59	3.99	8.37	1.91×10	3.8×10	7.25×10	1.32×10^{2}	2.3×10^{2}	3.65×10^{2}
M_v	17 1/2 to 18 1/2	18 1/2 to 19 1/2	19 1/2 to 20 1/2	20 1/2 to 21 1/2					
No/sq. deg.	6.45×10^{2}	1.03×10^{3}	1.12×10^{3}	1.62×10^{3}					

Assuming use of Electro-Optical System's RTT XY20B as a detector, the number of stars as a function of visual magnitude required to yield a unity S/N ratio for a 1 cylce bandwidth system employing 1/4 inch apertures in the star field reference was calculated and is summarized in Table III. The field of view required to provide the necessary number of stars is also summarized in Table III.

TABLE III

Number of Stars and Field of View for Unity S/N Ratio

M_v	Number of Stars	Field of View
0	2.65	4.19×10^4 sq. degrees
1	6.65	3.22×10^4
2	1.67×10	2×10^4
3	4.19×10	1.57×10^4
4	1.05×10^2	1.01×10^4
5	2.63×10^2	8.71×10^3
6	6.6×10^2	8.49×10^3
7	1.66×10^3	7.44×10^3
8	4.16×10^3	6.88×10^3
9	1.05×10^4	6.61×10^3
10	2.62×10^4	6.57×10^3
11	6.58×10^4	7.86×10^3

Admittedly, the data of Tables II and III (and also Table I) were derived by means of rough calculations and approximations. Their value, however, lies in the "feel" which they provide for the problem, thus opening new areas for investigation. As a result of the data of Tables II and III, for example, it becomes evident that image intensification is necessary in a feasible system design.

REFERENCES, APPENDIX B

[1] Russell, Dugan, Stewart; Astronomy II, Astrophysics and Stellar Astronomy; Ginn and Company, 1955.

APPENDIX C

SURVEY OF AMPLIFYING OPTICAL FRONT ENDS

An image intensifier tube usually associated with electronic light amplification is basically a multi-stage cascaded image converter using magnetic focusing of the electron image on a thin-film window to couple between stages. The thin-window coupling has phosphor on the first side and a photoemissive material on the second side so that the image is optically coupled with a minimum loss of light and image detail. It should be noted that the input cathode must be a photoemissive material, and as such is limited to shorter wavelength energy of less than 1.5 microns making it useful for sensing bodies which emit or reflect energy from black bodies approaching 4000°K. Thus it would not be applicable to sensing features on the dark side of planets, which is a limitation common to detectors employing photoemission such as photomultipliers. These image intensifiers have the advantage that the entire photoemitted image is accelerated, magnetically focused, and magnetically displaced in a manner such that the whole of the image is continuously available and may be subsequently optically correlated. Techniques for rotating the image electronically are not readily apparent; since each element must be displaced proportional to its radius from the center, a rather complex electromagnetic or electrostatic process would be required.

Newer techniques for image pickup and display employ solid state techniques. The image is sensed with a photo-conductor (PC) that is electrically coupled to an electroluminescent panel (EL) which displays the converted image. With proper spectral matching of the EL-PC, optical feedback may be employed. By selection of materials, impedances, and time constants, various memory conditions may be established. These techniques are presently limited in resolution. Librascope had developed materials which sense ultra-violet, display in the visible for up to ten minutes, and are erased by infrared. Resolutions of 5 line pairs/mm are possible with this technique as compared to 15 to 25 line pairs/mm for typical image intensifier tubes. (Phosphor currently being developed for typical tubes may yield 115 line pairs/mm, but the efficiency resolution product is about the same as for P-20 powder screens.)

A review of image intensifier techniques discloses a tremendous range of size and characteristics in these devices. Emphasis has been placed upon seeking a small intensifier, although versatility is also a major consideration. One of the smallest devices applicable to image intensification is the Bendix continuous-channel multiplier (Reference [1], pp. 211 and 219) which is a cylindrical tube 0.02 inches in diameter and 0.04 inches long. It is conceivable that an array of these small devices could be used as an intensifier, or that they could be arranged in groups to recognize a star pattern, although their application is presently limited by small aperture,

angle of incidence of the radiation, and sensitivity to ultraviolet. Because of its small size, some of the limitations of this tube may be overcome by coupling it optically to a small image converter tube like the RCA 6914 (1.75 inches in diameter and 2.75 inches long), thereby in effect achieving an optical aperture, or group of apertures that may be selected, similar to the electronic pinhole in an image dissector tube like the ITT 118 (2.0 inches in diameter and 6.25 inches long, with a cathode diameter of 0.75 inches).

Although the glass envelope of the image converter is more compact and the combination of components more versatile, a major difficulty may result in attempting to significantly deflect the image due to the greater photocathode diameter and accelerating potentials associated with the image converters and intensifiers. The accelerating potential of the RCA 6914 (Reference [2], p. 1604 and Reference [3]) is 16,000 volts for a conversion index of 30. Therefore, a low response deflection coil with many fine turns would appreciably increase the size and weight of the system. Tradeoffs between performance with lesser voltage gradients versus deflection requirements would need to be evaluated. This problem is common to wide photocathode image deflection systems where a high accelerating potential is relied upon for accurate focus and high efficiency-resolution product. Intensifiers which employ a sequential scan readout where a small interrogation beam originates from the neck of the tube are more easily controlled.

Devices which employ both the principles of image intensification and sequential scan readout such as the Intensifier Orthicon (Reference [1], p. 323) are excessively long (3.5 inches in diameter and 29 inches long). Their length is due to the fact that they are designed for low light levels such as +22 magnitude stars and, therefore, have high image intensification to overcome subsequent readout beam noise. Other devices which overcome readout beam noise by other means are the Isocon (Reference [1], p. 43) by subsequent multiplication of only the electrons scattered from the specularly reflected beam, and the Exitron (Reference [4], p. 306) which integrates the photoemitted image information before it is scanned. The Image Orthicon includes integration of the photoemitted image and also subsequent multiplication, and is consequently longer. Thus, there is a wide variety of tradeoffs between exceptional light amplification and simplicity in the image sensing device.

Gebel points out in Project Cateye (Reference [5], pp. 56 through 63) that an image converter does not increase contrast, and that

resolution is traded for sensitivity in cascading stages directly. Sequential light-amplification which has the ability to add and subsequently subtract information or to utilize derivative information may eliminate background, improve contrast, and sharpen edges, point sources, or moving targets (Reference [5], p. 58, Reference [1], p. 79 and Reference [6], p. 560). Simple background subtraction may be used to sharpen stationary edges and points by defocusing the subtracted image. This may be employed by subtracting alternate images (Reference [5], p. 57) sequentially, or to a limited extent by a balanced subtraction of one color from another (e.g., IR from UV) on a real time basis where the spectral characteristic of the background is known; however, backgrounds are seldom cooperative.

For horizon sensing against the earth, there exists a thermal gradient through the atmosphere and atmospheric windows through which the Earth itself may be sensed. These present a variety of criteria for distinguishing a particular horizon condition from false cloud reflections or some other portion of the gradient. The mean temperature of the upper atmosphere is about 220°K, with lows of about 205°K, such that a threshold of 200°K detected against a 4°K sky establishes a horizon in the upper atmosphere. This condition gives a peak radiation of 15μ with ground level radiation (through the 8-13μ window, peaking at 10μ) superimposed. Although many horizon scanners emphasize this upper atmosphere horizon in theory, a 200°K body does not radiate much energy and detectors are not very sensitive in this region so they actually rely upon the reinforcing energy through the 8-13μ window. This causes a vague horizon dependent upon relative contrast. The higher temperature of the Earth's surface radiates three to four times as much energy with a spectral peak in a region where detectors are more sensitive. Accurate horizon sensing at the Earth's surface depends upon sensing the contrast near the surface due to the adiabatic temperature gradient. The contrast between two temperatures over a narrow spectral band stands out most readily when contrast is sensed on the steep portion of the black body curve (Reference [4], p. 258) at wavelengths shorter than the spectral peak. When an observation of contrast is desirable, thermal imaging combined with techniques for contrast improvement offer interesting possibilities in viewing the Earth through the 3.0 to 4.0μ and/or 4.5 to 5.0μ atmospheric windows. The lower percent energy available in these limited regions is compensated for by a slope more applicable to sensing contrast, by more sensitive and versatile detectors, by a wider variety of optical materials and coatings, and by the ability to decrease radiation from surroundings by moderate cooling.

Infrared pickup tubes have various spectral response: (Reference [2], page 1607) and sensitivities depending upon the materials used. The more recent developments are classified and presented in the Proceedings of the Infrared Image Symposium. These image tubes also offer a compromise between star tracking of red stars over a broad spectral band, thermal sensing, and horizon sensing. Thus, sequential scanning and correlation offer the possibility of including the functions required for Earth-centered navigation. The dark side of a lunar orbit is more difficult in that the temperatures require sensing of 150°K, but there are tradeoffs in that the moon has no atmosphere and its radius is less, so a lesser angular accuracy may be required for equivalent orbital altitudes above the lunar surface.

REFERENCES, APPENDIX C

[1] Image Intensifier Symposium 1961, Fort Belvoir, Va.

[2] Proceedings of the IRE, September 1959.

[3] RCA Tube Manual

[4] W. A. Hiltner, Stars and Stellar Systems Volume II, II Astronomical Techniques; University of Chicago Press.

[5] ASTIA AD274028 Project Cateye.

[6] Proceedings of the IRE, May 1955.